Doubled Shapiro steps in a topological Josephson junction

Yu-Hang Li,[1] Juntao Song,[2] Jie Liu,[3,*] Hua Jiang,[4] Qing-Feng Sun,[1,5,6] and X. C. Xie[1,5,6]

[1]*International Center for Quantum Materials, School of Physics, Peking University, Beijing 100871, China*

[2]*Department of Physics and Hebei Advanced Thin Film Laboratory, Hebei Normal University, Shijiazhuang 050024, China*

[3]*Department of Applied Physics, School of Science, Xian Jiaotong University, Xian 710049, China*

[4]*College of Physics, Optoelectronics and Energy, Soochow University, Suzhou 215006, China*

[5]*Collaborative Innovation Center of Quantum Matter, Beijing 100871, China*

[6]*CAS Center for Excellence in Topological Quantum Computation, University of Chinese Academy of Sciences, Beijing 100190, China*

(Received 25 September 2017; revised manuscript received 6 December 2017; published 22 January 2018)

We study the transport properties of a superconductor–quantum spin Hall insulator–superconductor hybrid system in the presence of microwave radiation. Instead of adiabatic analysis or use of the resistively shunted junction model, we start from the microscopic Hamiltonian and calculate the d.c. current directly with the help of the nonequilibrium Green's function method. The numerical results show that (i) the *I*-*V* curves of background current due to multiple Andreev reflections exhibit a different structure from those in the conventional junctions, and (ii) all Shapiro steps are visible and appear one by one at high frequencies, while at low frequencies, the steps evolve exactly as the Bessel functions and the odd steps are completely suppressed, implying a fractional Josephson effect.

DOI: 10.1103/PhysRevB.97.045423

I. INTRODUCTION

The Majorana bound state (MBS), which harbors non-Abelian statistics, has recently attracted extensive interest for its potential applications in fault-tolerant topological quantum computation [1–5]. The realization of these states was first expected theoretically by Kitaev in a one-dimensional spinless p-wave superconducting chain [6]. Unfortunately, despite that p-wave pairing is scarce in nature due to spin degeneracy, the inevitable "Majorana fermion doubling problem" [46] made it impossible to realize in experiments [7–9]. Soon afterward, many schemes for engineering Kitaev's ideal model in condensed material systems were put into practice [10–15]. A conceptual breakthrough came in 2009 when Fu and Kane proved that topological junctions between superconductors mediated by a quantum spin Hall insulator (QSHI) can stabilize those MBSs at their interfaces [16]. In this system, effective p-wave pairing can be achieved by superconducting proximity effects combined with time-reversal symmetry breaking. Furthermore, the Majorana fermion doubling problem is automatically circumvented because there exists only one pair of Fermi points as long as the Fermi level does not intersect the bulk bands. In addition, MBSs are also proposed to exist in other systems, for example, as quasiparticle excitations of the quantum Hall state at filling factor $\nu = 5/2$ [17,18], in the vortices of the intrinsic p-wave superconductor Sr_2RuO_4 [19], and in cold-atom systems [20,21].

Experimental probes of these MBSs can be achieved by measurement of the fractional Josephson effect [22–24]. The coupling of two MBSs γ_1 and γ_2 localized at the interfaces of a topological Josephson junction allows the tunneling of half Fermion pairs and, in turn, yields a 4π periodic supercurrent $I_{4\pi}\sin(\phi/2)$, namely, the fractional Josephson effect. As a result, in the presence of a d.c. bias voltage V_0, one would expect an a.c. Josephson current at half Josephson frequency $\omega_0/2 = eV_0/\hbar$ accompanied by radio-frequency radiation of the same frequency [25–28]. Moreover, supplementing the junction with a radio-frequency emission of frequency ω, a current measurement will find plateaus of the voltage steps, also known as Shapiro steps, emerging only when $2eV_0/\hbar = 2n\omega$ [26,27,29–31], where n is an integer, leading to an even-odd effect with all odd steps disappeared. A second type of fractional Josephson effect, which exhibits 4π periodicity in both superconducting phases of the left and right leads, may arise if the barrier material in the Josephson junction is also a superconductor [22,32]. Some recent experiments were performed to explore this even-odd effect in superconductor–quantum spin Hall insulator–superconductor S-QSHI-S Josephson junctions [33,34] and several other systems [35,36] which are believed may hold MBSs. Interestingly, the results show a strong frequency dependence. Thus far, only the resistively shunted junction model has been considered to understand this effect [37]. Under this approach, the system is simplified as a circuit with a Josephson junction shunted by a resistance R, which can be described by an equation of motion: $I_0 + I_{\text{a.c.}}\sin(\omega t) = V/R + I(\phi)$. The 4π periodic term $I(\phi) = I_{4\pi}\sin(\phi/2)$ in this equation phenomenologically leads to an even-odd effect in Shapiro steps. However, a microscopic mechanism of the direct connection between the presence of MBSs and this even-odd effect is lacking, and the underlying physics of this effect's being exhibited only at low frequencies in experiments need to be understood.

In this paper, we study the transport properties of an S-QSHI-S Josephson junction. Using the nonequilibrium Green's function method, we calculate the tunneling current based

*jieliuphy@mail.xjtu.edu.cn

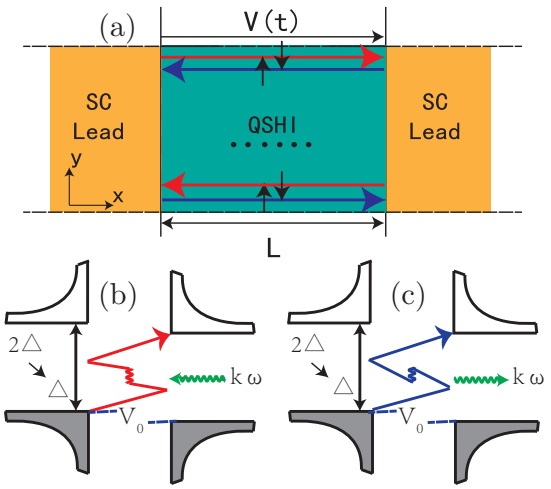

FIG. 1. (a) Schematic for the S-QSHI-S device with voltage $V(t) = V_0 + V_1 \sin(\omega t)$. (b, c) Schematics for three-order MAR mediated by absorbing or emitting k photons, respectively.

on a tight-binding Hamiltonian. Our numerical results show that the I-V curves of the background currents exhibit an interesting subharmonic gap structure, which is caused by the multiple Andreev reflections (MARs). Differently from the conventional Josephson junctions, the presence of MBSs reduces the gap from 2Δ to Δ, and therefore, the I-V curves have singularities at voltages $eV_0 = (\Delta \mp k\hbar\omega)/n$ rather than $eV_0 = (2\Delta \mp k\hbar\omega)/n$, with n, k being integer numbers. On the other hand, we find that the Shapiro steps appear one by one and have complicated oscillation patterns at higher frequencies due to the nonadiabatic process. However, at low frequencies, the steps evolve exactly as the Bessel functions but with the odd steps suppressed strongly, in agreement with the recent experimental results in Ref. [34].

The rest of this paper is organized as follows. In Sec. II, we introduce our model Hamiltonian and deduce the equation of the supercurrent by virtue of the nonequilibrium Green's function method. In Sec. III, we focus our results on the d.c. current and study the background current and the Shapiro steps in detail. Finally, a brief summary is presented in Sec. IV.

II. MODEL AND FORMALISM

We consider a voltage biased S-QSHI-S Josephson junction in the presence of microwave radiation as shown in Fig. 1(a). To proceed, this external field is simulated with a time-dependent voltage $V(t) = V_0 + V_1 \sin(\omega t)$. Then after a unitary transformation [38], the system can be described by the following Hamiltonian:

$$\mathcal{H} = \sum_{\alpha=L,R} \mathcal{H}_\alpha(t) + \mathcal{H}_C + \mathcal{H}_T. \tag{1}$$

Here, $\mathcal{H}_\alpha(\alpha = L,R) = \sum_{k,\sigma} \epsilon_{\alpha k} a^\dagger_{\alpha k\sigma} a_{\alpha k\sigma} + \Delta(a_{\alpha k\downarrow} a_{\alpha -k\uparrow} + \text{H.c.})$ are the BCS Hamiltonians of both the left and the right s-wave superconducting leads, where $a^\dagger_{\alpha k\sigma}(a_{\alpha k\sigma})$ are the creation (annihilation) operators of electrons in the α lead with momentum k and spin σ, $\epsilon_{\alpha k}$ is the kinetic energy, and Δ is the common superconducting energy gap shared by both leads. As the transport properties are dominated by the helical edge states of the central QSHI [39,40], this part can be described by an effective one-dimensional Hamiltonian [41], which in the Nambu representation is $\mathcal{H}_C = \frac{-iV_F}{2a}\Psi_i^\dagger \sigma_z \tau_z \Psi_{i+\delta x} - \mu \Psi_i^\dagger \tau_z \Psi_i + M \Psi_i^\dagger \sigma_x \Psi_i$. a is the lattice constant, $\Psi_i^T = [\psi_{i\uparrow}, \psi_{i\downarrow}, \psi^\dagger_{i\downarrow}, -\psi^\dagger_{i\uparrow}]$ are the edge states, V_F and μ are the velocity and the chemical potential of the edge states, M is the Zeeman energy caused by an external magnetic field, and σ_j and τ_j are the Pauli matrices acting in the spin and Nambu spaces, respectively. The last term in Eq. (1), representing the time-dependent coupling between the superconducting leads and the central part, has the form $\mathcal{H}_T = \sum_\alpha (a^\dagger_{\alpha k\uparrow}, a_{\alpha k\downarrow}) \mathbf{t}_{\alpha C} \Psi_i + \text{H.c.}$ The coupling matrix $\mathbf{t}_{\alpha C}(t) = \begin{pmatrix} \tilde{t}_\alpha & \tilde{t}_\alpha & 0 & 0 \\ 0 & 0 & -\tilde{t}^*_\alpha & -\tilde{t}^*_\alpha \end{pmatrix}$, where $\tilde{t}_\alpha = t_c \exp\{i[\phi_\alpha/2 + z_\alpha t + p_\alpha \cos(\omega t)]\}$, with t_c the coupling strength, $\phi_{L,R}$ the initial superconducting phases of the left and right leads, $z_\alpha = eV_0^\alpha/\hbar$ the d.c. voltage, and $p_\alpha = eV_1^\alpha/\hbar\omega$ the radiation power. In fact, by making a unitary transformation with $\tilde{a}^\dagger_{\alpha k\uparrow/\downarrow} = \frac{\sqrt{2}}{2}(a^\dagger_{\alpha k\uparrow/\downarrow} \pm a^\dagger_{\alpha k\downarrow/\uparrow})$, $\mathcal{H}_T$ can reduce to $\mathcal{H}_T = \sqrt{2}\tilde{t}_\alpha \tilde{a}^\dagger_{\alpha k\sigma} \psi_{i\sigma} + \text{H.c.}$, the same as for the normal barriers.

The total current from the left superconducting lead can be calculated from the evolution of the electron number operator $N_L = \sum_{k\sigma} a^\dagger_{Lk\sigma} a_{Lk\sigma}$ in that lead,

$$I_L(t) = -e\left\langle \frac{dN_L}{dt} \right\rangle = \frac{ie}{\hbar}\left\langle \left[\sum_{k,\sigma} a^\dagger_{Lk\sigma} a_{Lk\sigma}, \mathcal{H} \right] \right\rangle$$
$$= \frac{e}{\hbar} \text{Tr}[\Gamma_z \mathbf{G}^<_{CL}(t,t) \mathbf{t}_{LC} + \text{H.c.}], \tag{2}$$

where $\Gamma_z = \sigma_z \bigotimes \mathbf{I}_2$, with $\mathbf{I}_2$ the 2×2 identity matrix, and $\mathbf{G}^<_{CL}(t,t)$ is the distribution Green's function, which satisfies the relation $\mathbf{G}^<_{CL}(t,t) = \int dt_1 [\mathbf{G}^r(t,t_1) \mathbf{t}^\dagger_{LC} \mathbf{g}^<_L(t_1,t) + \mathbf{G}^<(t,t_1) \mathbf{t}^\dagger_{LC} \mathbf{g}^a_L(t_1,t)]$. $\mathbf{g}^{<,a}_L(t_1,t_2)$ are the surface Green's functions of the uncoupled superconducting lead, and $\mathbf{G}^{r,<}(t_1,t_2)$ are the retarded and distribution Green's functions of the central QSHI part. For convenience, we take the left superconducting lead as the potential ground. Thus the current can be rewritten as

$$I_L(t) = \frac{2e}{\hbar} \text{Im} \int_{-\infty}^{t} dt_1 \int \frac{d\epsilon}{2\pi} e^{i\epsilon(t-t_1)} \text{Tr}$$
$$\times \left\{ \Gamma_z \left[\mathbf{G}^r(t,t_1) \times \Sigma^<_L(\epsilon) + \mathbf{G}^<(t,t_1) \Sigma^a_L(\epsilon) \right] \right\}, \tag{3}$$

where $\Sigma^{<,a}_L(\epsilon) = \mathbf{t}^\dagger_{LC} \mathbf{g}^{<,a}_L(\epsilon) \mathbf{t}_{LC}$ are the distribution and retarded self-energies due to coupling to the left superconducting lead. The exact retarded Green's functions of the uncoupled superconducting lead read $\mathbf{g}^r_{L,R}(\epsilon) = 2\pi\rho\beta(\epsilon)[\mathbf{I}_2 + \Delta/\epsilon\sigma_x]$, where the corresponding BCS density of states $\beta(\epsilon)$ is defined as $\beta(\epsilon) = \epsilon/(i\sqrt{\Delta^2 - \epsilon^2})$ for $\Delta > |\epsilon|$ and $\beta(\epsilon) = |\epsilon|/\sqrt{\epsilon^2 - \Delta^2}$ for $\Delta < |\epsilon|$. In addition, the normal density of states ρ is assumed to be independent of the energy ϵ. The advanced Green's functions $\mathbf{g}^a_{L,R}$ are the complex conjugates of the retarded Green's function and $\mathbf{g}^<_{L,R} = f(\epsilon)(\mathbf{g}^a_{L,R} - \mathbf{g}^r_{L,R})$, where $f(\epsilon) = 1/(1 + e^{\epsilon/k_B T})$ is the Fermi distribution function.

In order to obtain the Green's function, following the method in Ref. [42], we perform a Fourier transform

with respect to the temporal arguments, $\mathbf{G}(t_1,t_2) = 1/2\pi \int d\epsilon_1 \int d\epsilon_2 e^{-i\epsilon_1 t_1} e^{i\epsilon_2 t_2} \mathbf{G}(\epsilon_1,\epsilon_2)$. Because the phase difference of the junction is a time-dependent periodic function with two periods, $T_1 = 2\pi/\omega_0$ and $T_2 = 2\pi/\omega$, where $\omega_0 = 2e|V_0|$, $\mathbf{G}(\epsilon_1,\epsilon_2)$ satisfies the following relation: $\mathbf{G}(\epsilon_1,\epsilon_2) = \sum_{m,n} \mathbf{G}(\epsilon_1,\epsilon_1 + m\omega_0 + n\omega)\delta(\epsilon_2 - \epsilon_1 - m\omega_0 - n\omega)$, where m, n are integer numbers. To simplify the mathematical expression of the supercurrent, we introduce the quantities $\mathbf{G}^{kl}_{mn} \equiv \mathbf{G}(\epsilon + m\omega_0 + k\hbar\omega, \epsilon + n\omega_0 + l\hbar\omega)$. Finally, the current can now be expanded as $I(t) = \sum_{n,m} I_n^m \exp[i(n\omega_0 t + m\omega t)]$, where the current amplitudes I_n^m can be expressed as

$$I_n^m = \frac{2e}{\hbar}\mathrm{Im}\int \frac{\mathrm{d}\epsilon}{2\pi}\mathrm{Tr}\big\{\Gamma_z\big[\mathbf{G}^{r;-m0}_{-n0}(\epsilon)\Sigma_L^<(\epsilon) + \mathbf{G}^{<;-m0}_{-n0}(\epsilon)\Sigma_L^a(\epsilon)\big]\big\}. \tag{4}$$

At this point, the calculation of the supercurrent has been reduced to the calculation of the Fourier components of the retarded and distribution Green's functions, which can be determined by numerically solving the Dyson equation and the Keldysh equation,

$$\mathbf{G}^{r;kl}_{mn} = \mathbf{g}^{r;k}_m \delta_{mn}\delta_{kl} + \sum_{i,j} \mathbf{G}^{r;kj}_{mi}\Sigma^{r;jl}_{in} g^{r;l}_n, \tag{5a}$$

$$\mathbf{G}^{<;kl}_{mn} = \sum_{i_1,i_2,j_1,j_2} \mathbf{G}^{r;kj_1}_{mi_1}\Sigma^{<;j_1 j_2}_{i_1 i_2}\mathbf{G}^{a;j_2 l}_{i_2 n}, \tag{5b}$$

where $\mathbf{g}^{r;k}_m = \mathbf{g}^r(\epsilon + m\omega_0 + k\omega)$ and $\Sigma^{r,<;kl}_{mn} = \Sigma^{r,<;kl}_{L;mn} + \Sigma^{r,<;kl}_{R;mn}$. The Fourier components of the self-energies $\Sigma^{r,<;kl}_{L,R;mn}$ adopt the forms

$$\Sigma^{r;kl}_{L;nm} = -i\pi t_c^2 \beta_n^k \Sigma_L\big(\epsilon_n^k\big)\delta_{nm}\delta_{kl}, \tag{6a}$$

$$\Sigma^{r;kl}_{R;nm} = -i\pi t_c^2 \sum_j J_{k-j}(p)J_{j-l}(p)\begin{pmatrix} (-1)^j i^{-k-l}\beta^j_{n+1/2}\delta_{nm} & -i^{k-l}\beta^j_{n+1/2}\frac{\Delta}{\epsilon^j_{n+1/2}}e^{-i\phi_R}\delta_{n,m-1} \\ i^{l-k}\beta^j_{n-1/2}\frac{\Delta}{\epsilon^j_{n-1/2}}e^{i\phi_R}\delta_{n,m+1} & (-1)^j i^{k+l}\beta^j_{n-1/2}\delta_{nm}\end{pmatrix}\bigotimes \mathbf{M}, \tag{6b}$$

$$\Sigma^{<;kl}_{L;nm} = 2i\pi t_c^2 \gamma_n^k \Sigma_L\big(\epsilon_n^k\big)\delta_{nm}\delta_{kl}, \tag{7a}$$

$$\Sigma^{<;kl}_{R;nm} = 2i\pi t_c^2 \sum_j J_{k-j}(p)J_{j-l}(p)\begin{pmatrix} (-1)^j i^{-k-l}\gamma^j_{n+1/2}\delta_{nm} & -i^{k-l}\gamma^j_{n+1/2}\frac{\Delta}{\epsilon^j_{n+1/2}}e^{-i\phi_R}\delta_{n,m-1} \\ i^{l-k}\gamma^j_{n-1/2}\frac{\Delta}{\epsilon^j_{n-1/2}}e^{i\phi_R}\delta_{n,m+1} & (-1)^j i^{k+l}\gamma^j_{n-1/2}\delta_{nm}\end{pmatrix}\bigotimes \mathbf{M}, \tag{7b}$$

where $\epsilon_n^k = \epsilon + n\omega_0 + k\omega$, $\beta_i^j = \beta(\epsilon + i\omega_0 + j\omega)$, $\gamma_i^j = f_i^j \beta_i^j$, $\mathbf{M} = \sigma_0 + \sigma_x$, and $J_n(p)$ is the first kind of Bessel function of order n, with $p = p_R - p_L$ denoting the radiation power. Finally, the time-dependent supercurrent can be calculated without further complications.

III. RESULTS AND DISCUSSION

In this paper, we focus on the d.c. current, which consists of two parts: the background current I_0^0 and the Shapiro steps I_n^m. Note that the Shapiro steps depend on the average value of the initial phase difference $\phi_0 = \phi_R - \phi_L$. In the following, we take the superconducting energy gap Δ as the energy unit. The parameters of the central Hamiltonian are $a = 5$ nm, $L = 100$ nm, $\hbar V_F = 200\Delta$, $M = 1.5\Delta$, and $\mu = 0$ so all energies are measured from the chemical potential. The coupling strength between the central QSHI part and the superconducting leads takes $t_c = 1.8\Delta$ and the temperature is set as 0 in our detailed calculations. Here, the transmission probability is defined as $D = 1/[1 + \sinh^2(ML)]$ [16]. We fix the system parameters unless otherwise specified.

Let us start by analyzing the background current. The key feature of the background current is that its I-V curves have some singularities at discrete voltages $eV_0 = (2\Delta \mp k\hbar\omega)/n$, which originates from an n-order MAR mediated by absorbing [Fig. 1(b)] or emitting [Fig. 1(c)] k photons with their probabilities proportional to $J_k(p)$ [42]. After this photoassisted MAR process, a quasiparticle acquires the energy $neV \pm k\hbar\omega$, and singularities appear simultaneously when this energy can overcome the energy gap 2Δ between the occupied and the empty states. However, in topological Josephson junctions, because of the presence of the MBSs, the energy gap reduces to Δ, and thus singularities should appear at $eV_0 = (\Delta \mp k\hbar\omega)/n$ instead [26,43].

In Fig. 2, we plot the I-V curves of the background current with different radiation power p and frequency ω. It can be clearly seen that when $p = 0$ (red line), which means in the absence of microwave radiations, the curve exhibits gap structures at voltages $eV_0 = \Delta/n$, while with microwave radiation added, the curves show rich subgap structures with more singularities appearing at $eV = (\Delta \mp k\hbar\omega)/n$ (see the sign $eV_0 = 0.75$ of the lime-green line with $p = 1.0$, $\omega = 0.25$). This distinct structure strongly indicates the presence

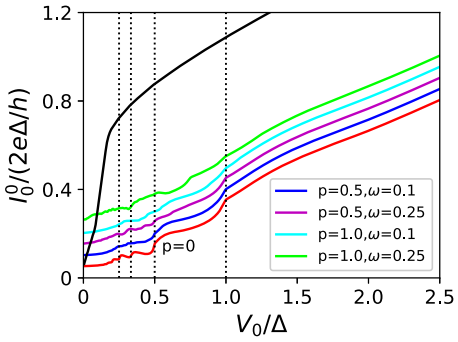

FIG. 2. Background current I_0^0 as a function of the d.c. voltage V_0 with different parameters. Colorful curves are displayed to make the figure clear. Red curve, the case $p = 0$; black curve, $M = 0, p = 0$. Here, $\phi_L = \phi_R = 0$.

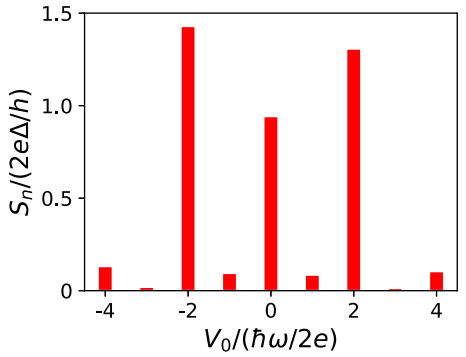

FIG. 3. Bar plots of the heights of the Shapiro steps S_n from $n = -4$ to $n = 4$ at frequency $\omega = 0.02\Delta$. Here, the radiation power is $p = \Delta$.

of MBSs. Note that the black curve in Fig. 2 corresponds to the case of $M = 0$ and $p = 0$, in which the junction is like a conventional one due to the lack of localized MBSs. Naturally, because of the conducting helical edge, this junction is totally transparent with the transmission probability $D = 1$, leading to a sharply increasing I-V curve as plotted in the figure [44].

Now we move on to the Shapiro steps. These steps, arising from the phase locking between the harmonics of the a.c. Josephson frequency ω_0 and the microwave radiation frequency ω, have been reported extensively in conventional Josephson junctions. Within an adiabatic approximation [45], these steps can be understood as a consequence of the non-sinusoidal current-phase relation. As stated above, the phase difference across the junction is $\phi(t) = \phi_0 + zt + p\sin(\omega t)$. Substituting this into Josephson's first equation and using the standard mathematical expansion of a sine in terms of the Bessel functions, one would expect the Shapiro steps to evolve exactly as $J_n(2p)$ and to appear at $z = n\omega$, where n is an integer. In principle, the situations are different between conventional and topological Josephson junctions. In a conventional one, because the only carriers that are permitted to transmit through the central insulator part are Cooper pairs, Shapiro steps appear at $V_0 = n\hbar\omega/2e$ with $z = 2eV_0$. However, in a topological one, two MBSs, γ_1 and γ_2, are localized separately at the interfaces of the superconducting leads and the central QSHI region [16]. Their strong coupling forms a 4π fractional Josephson effect and allows the tunneling of single electrons, therefore Shapiro steps can appear at double the voltage of the former one and exhibit an even-odd effect when $z = eV_0$ as plotted in Fig. 3. Here, the heights of the Shapiro steps are defined as $S_n \equiv |I_n^1|$. It should be pointed out that the fractional Shapiro steps I_n^m with $m > 1$ are so small in our calculations that we have omitted them from the figure. Interestingly, the absence of the odd steps here is not calculated by simply adding a 4π supercurrent in the RSJ model but the direct result of the nonequilibrium Green's function method based on the intrinsic Hamiltonian. Besides, this fundamental method can help us to further understand the frequency dependence of the even-odd effect.

In Fig. 4, we display the heights of the first five Shapiro steps S_n as the increase in the radiation powers at three frequencies: $\omega = 0.02$, $\omega = 0.05$, and $\omega = 0.5$. As illustrated in Fig. 4(a), the Shapiro steps coincide well with the Bessel functions except that the odd ones are strongly suppressed at

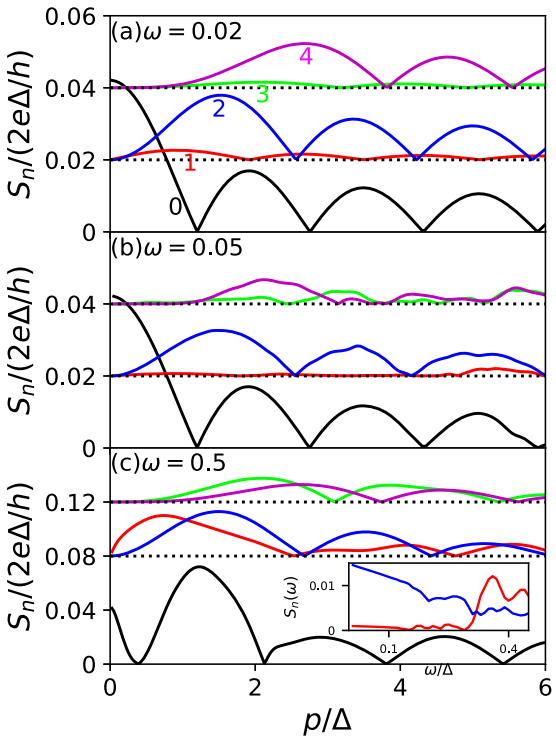

FIG. 4. Heights of the first five Shapiro steps S_n versus the radiation power p at three frequencies: (a) $\omega = 0.02$, (b) $\omega = 0.05$, and (c) $\omega = 0.5$. Here, some steps are vertical shifted for clarity. Inset: S_1 (red line) and S_2 (blue line) as the increase in the frequency with radiation power $p = \Delta$.

frequency $\omega = 0.02$, leading to an even-odd effect as predicted and reported in some recent works [26,27,33,34]. With the frequency increased to $\omega = 0.05$, Fig. 4(b) shows that although the first step is still heavily suppressed, higher order steps begin to appear. As a comparison, we plot the heights S_n at a high frequency, $\omega = 0.5$, in Fig. 4(c). Though the shapes deviate seriously from Bessel functions, all steps are visible and appear one by one as the increase in the radiation power. In general, the deviation results from a nonadiabatic process at high frequencies. The inset shows the heights S_1 and S_2 as the increase in the frequency ω. We can clearly see that S_1 is suppressed heavily when $\omega < 0.3\Delta$, which indicates that the even-odd effect can only be seen at low frequencies. The reason is that the Andreev bound state may couple the continuum after absorbing a large frequency radiation, restoring a 2π periodicity. For superconducting leads made of Al electrodes, our results are in general agreement with the experiment data in Ref. [34] if the time-reversal symmetry is implicitly broken since the frequencies here are about $\omega = 0.5$ GHz [Fig. 4(a)], $\omega = 1.2$ GHz [Fig. 4(b)], and $\omega = 12$ GHz [Fig. 4(c)]. The exact mechanism for the seemingly perfect transmission in that work remains to be understood.

IV. SUMMARY

To summarize, we have studied the transport properties of an S-QSHI-S Josephson junction in the presence of microwave radiation. Using nonequilibrium Green's functions, we calculate the d.c. supercurrent at an arbitrary frequency starting from

the initial tight-binding Hamiltonian. The distinct singularities of the background current prove that the presence of MBSs reduces the gap from 2Δ to Δ. Furthermore, the even-odd effect of the Shapiro steps can only be seen at low frequencies. Our theory provides a good explanation of the connection between the even-odd effect and the MBSs.

ACKNOWLEDGMENTS

This work was supported by the NBRPC (Grants No. 2015CB921102 and No. 2014CB920901), the National Key R and D Program of China (2017YFA0303301), the NSF-China under Grants No. 11574007, No. 11574245, and No. 11534001, the Key Research Program of the Chinese Academy of Sciences (Grant No. XDPB08-4), and the NSF of Jiangsu Province, China (Grant No. BK20160007).

APPENDIX A

In this Appendix, we present a numerical method for solving the Dyson equation [Eq. (5a)] in Sec. II above. In general, this equation can be solved literally. However, the process is very time-consuming. Inspired by the solution of the linear polynomial, we find that this equation can be solved similarly. Because the index in that equation can be any infinite large integer, cutoffs are necessary before we solve it. We assume that the lower index $-L \leqslant m,n \leqslant L$ and the upper index $-U \leqslant k,l \leqslant U$. Then the Dyson equation can be rewritten as

$$\mathbf{G}^r_{ij} = \mathbf{g}^r_{ij}\delta_{ij} + \sum_{i'} \mathbf{G}^r_{ii'}\Sigma^r_{i'j}\mathbf{g}^r_{jj}, \tag{A1}$$

where $i = mU + k$, $j = nU + l$, and i' denotes the summation from $-LU$ to LU. For a certain i, we replace the matrices above as $\mathbf{X}_{i'} = \mathbf{G}^r_{ii'}$, $\mathbf{A}_{i'j} = \delta_{i'j} - \Sigma^r_{i'j}\mathbf{g}^r_{jj}$, and $\mathbf{B}_{i'j} = \mathbf{g}^r_{i'j}\delta_{i'j}$. Equation (A1) can be equally written as

$$\hat{\mathbf{X}}^T\hat{\mathbf{A}} = \hat{\mathbf{B}}, \tag{A2}$$

where a hat denotes an array. Noting that every element in the array in Eq. (A2) is also a matrix, $\hat{\mathbf{X}}$ can finally be obtained by block diagonalizing the array $\hat{\mathbf{A}}$.

APPENDIX B

In this Appendix, we show the transmission probability dependence of the even-odd effect. As stated above, the transmission probability is defined as $D = 1/[1 + \sinh^2(ML)]$, where M is the Zeeman energy and L is the length of the central QSHI region. Since we fix the system length as $L =$ 100 nm, different Zeeman energies can be used to represent different transmission probabilities. In general, the fractional Josephson effect can be seen easily with a low transmission probability or, equally, a high Zeeman energy. In Fig. 5, we display the background current I^0_0 versus the d.c. voltage V_0 at different Zeeman energies with $p = 0$. All currents exhibit gap structures at voltages $eV_0 = \Delta/n$, with n an integer. Moreover, the structure can be seen more clearly as the increase in the Zeeman energy, which corresponds to the decrease in the transmission probability. This distinct structure strongly indicates that the superconducting gap is reduced from 2Δ to Δ, which is in very good agreement with the result in the text.

In the experiment reported in [34], the transmission probability seems to be $D = 1$ since the time-reversal symmetry

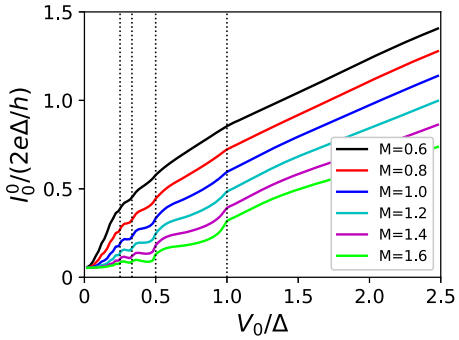

FIG. 5. Background current I^0_0 as a function of the d.c. voltage V_0 at different Zeeman energies which correspond to different transmission probabilities without any radio-frequency radiation. Here, the other parameters are the same as in Fig. 2.

is not explicitly broken. Theoretically, the supercurrent will restore a 2π periodicity due to a perfect transmission. Nevertheless, the experimental data contradict the existing theoretical proposals. In order to study this paradox, we show the heights of the first five Shapiro steps S_n versus the increase in the radiation power p at two transmission probabilities, $M = 0$ [Fig. 6(a)] and $M = 1.2\Delta$ [Fig. 6(b)]. As is clearly shown, the odd steps are only suppressed at $M_z = 1.2\Delta$, which corresponds to a fractional transmission probability but different from that in the text, while at $M_z = 0$, or equally $D = 1$, all Shapiro steps are visible. This result generally agrees with the theoretical works but also contradicts the experiment data. The reason may be that the time-reversal symmetry in the experiment is implicitly broken by some other effects such as puddles [28]. However, the exact mechanism still needs to be studied further.

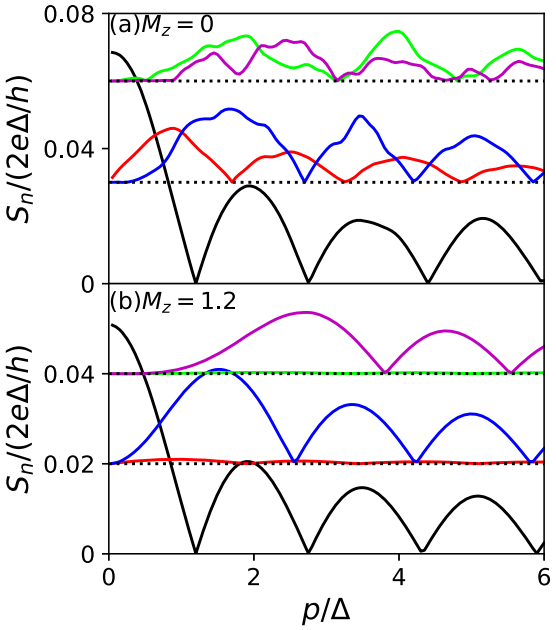

FIG. 6. Heights of the first five Shapiro steps S_n versus the radiation power p at two transmission probabilities, (a) $M_z = 0$ and (b) $M_z = 1.2\Delta$. Here, the frequency is taken as $\omega = 0.02$, and the other parameters are the same as in Fig. 4.

[1] A. Stern, Nature **464**, 187 (2010).

[2] C. Nayak, S. H. Simon, A. Stern, M. Freedman, and S. Das Sarma, Rev. Mod. Phys. **80**, 1083 (2008).

[3] A. Kitaev, Ann. Phys. **303**, 2 (2003).

[4] S. Das Sarma, M. Freedman, and C. Nayak, Phys. Rev. Lett. **94**, 166802 (2005).

[5] P. Bonderson, M. Freedman, and C. Nayak, Phys. Rev. Lett. **101**, 010501 (2008).

[6] A. Y. Kitaev, Phys. Usp. **44**, 131 (2001).

[7] L. Fidkowski and A. Kitaev, Phys. Rev. B **81**, 134509 (2010).

[8] L. Fidkowski and A. Kitaev, Phys. Rev. B **83**, 075103 (2011).

[9] Y. Niu, S. B. Chung, C.-H. Hsu, I. Mandal, S. Raghu, and S. Chakravarty, Phys. Rev. B **85**, 035110 (2012).

[10] L. Fidkowski, R. M. Lutchyn, C. Nayak, and M. P. A. Fisher, Phys. Rev. B **84**, 195436 (2011).

[11] J. D. Sau, B. I. Halperin, K. Flensberg, and S. Das Sarma, Phys. Rev. B **84**, 144509 (2011).

[12] L. Fu and C. L. Kane, Phys. Rev. Lett. **100**, 096407 (2008).

[13] R. M. Lutchyn, J. D. Sau, and S. Das Sarma, Phys. Rev. Lett. **105**, 077001 (2010).

[14] Y. Oreg, G. Refael, and F. von Oppen, Phys. Rev. Lett. **105**, 177002 (2010).

[15] A. Cook and M. Franz, Phys. Rev. B **84**, 201105 (2011).

[16] L. Fu and C. L. Kane, Phys. Rev. B **79**, 161408 (2009).

[17] G. Moore and N. Read, Nucl. Phys. B **360**, 362 (1991).

[18] N. Read and D. Green, Phys. Rev. B **61**, 10267 (2000).

[19] S. Das Sarma, C. Nayak, and S. Tewari, Phys. Rev. B **73**, 220502 (2006).

[20] V. Gurarie, L. Radzihovsky, and A. V. Andreev, Phys. Rev. Lett. **94**, 230403 (2005).

[21] S. Tewari, S. Das Sarma, C. Nayak, C. Zhang, and P. Zoller, Phys. Rev. Lett. **98**, 010506 (2007).

[22] J. Alicea, Rep. Prog. Phys. **75**, 076501 (2012).

[23] C. Beenakker, Annu. Rev. Condens. Matter Phys. **4**, 113 (2013).

[24] Y. Peng, F. Pientka, E. Berg, Y. Oreg, and F. von Oppen, Phys. Rev. B **94**, 085409 (2016).

[25] S.-P. Lee, K. Michaeli, J. Alicea, and A. Yacoby, Phys. Rev. Lett. **113**, 197001 (2014).

[26] D. M. Badiane, M. Houzet, and J. S. Meyer, Phys. Rev. Lett. **107**, 177002 (2011).

[27] P. San-Jose, E. Prada, and R. Aguado, Phys. Rev. Lett. **108**, 257001 (2012).

[28] R. S. Deacon, J. Wiedenmann, E. Bocquillon, F. Domínguez, T. M. Klapwijk, P. Leubner, C. Brüne, E. M. Hankiewicz, S. Tarucha, K. Ishibashi *et al.*, Phys. Rev. X **7**, 021011 (2017).

[29] F. Domínguez, F. Hassler, and G. Platero, Phys. Rev. B **86**, 140503 (2012).

[30] J. Picó-Cortés, F. Domínguez, and G. Platero, Phys. Rev. B **96**, 125438 (2017).

[31] J. D. Sau and F. Setiawan, Phys. Rev. B **95**, 060501 (2017).

[32] L. Jiang, D. Pekker, J. Alicea, G. Refael, Y. Oreg, and F. von Oppen, Phys. Rev. Lett. **107**, 236401 (2011).

[33] J. Wiedenmann, E. Bocquillon, R. S. Deacon, S. Hartinger, O. Herrmann, T. M. Klapwijk, L. Maier, C. Ames, C. Brüne, and C. Gould, Nat. Commun. **7**, 10303 (2016).

[34] E. Bocquillon, R. S. Deacon, J. Wiedenmann, P. Leubner, T. M. Klapwijk, C. Brüne, K. Ishibashi, H. Buhmann, and L. W. Molenkamp, Nat. Nanotechnol. **12**, 137 (2016).

[35] L. P. Rokhinson, X. Liu, and J. K. Furdyna, Nat. Phys. **8**, 795 (2012).

[36] C. Li, J. C. de Boer, B. de Ronde, S. V. Ramankutty, E. van Heumen, Y. Huang, A. de Visser, A. A. Golubov, M. S. Golden, and A. Brinkman, arXiv:1707.03154.

[37] F. Domínguez, O. Kashuba, E. Bocquillon, J. Wiedenmann, R. S. Deacon, T. M. Klapwijk, G. Platero, L. W. Molenkamp, B. Trauzettel, and E. M. Hankiewicz, Phys. Rev. B **95**, 195430 (2017).

[38] Q.-F. Sun, B.-g. Wang, J. Wang, and T.-h. Lin, Phys. Rev. B **61**, 4754 (2000).

[39] J. Song, H. Liu, J. Liu, Y. X. Li, R. Joynt, Q. F. Sun, and X. C. Xie, Phys. Rev. B **93**, 195302 (2016).

[40] S. Hart, H. Ren, T. Wagner, P. Leubner, M. Mühlbauer, C. Brüne, H. Buhmann, L. W. Molenkamp, and A. Yacoby, Nat. Phys. **10**, 638 (2014).

[41] Y.-F. Zhou, H. Jiang, X. C. Xie, and Q.-F. Sun, Phys. Rev. B **95**, 245137 (2017).

[42] J. C. Cuevas, J. Heurich, A. Martín-Rodero, A. Levy Yeyati, and G. Schön, Phys. Rev. Lett. **88**, 157001 (2002).

[43] P. San-Jose, J. Cayao, E. Prada, and R. Aguado, New J. Phys. **15**, 075019 (2013).

[44] J. C. Cuevas, A. Martín-Rodero, and A. Levy Yeyati, Phys. Rev. B **54**, 7366 (1996).

[45] N. Kopnin, *Introduction to The Theory of Superconductivity* (Cryocourse, Helsinki, 2009).

[46] Suppose the spinless fermions are replaced with spinful ones. In this case each end of the Kiteav chain supports two Majorana zero modes or, equally, an ordinary fermionic zero mode, the energy of which will move away from 0 due to some inevitable effects such as spin-orbital coupling.